Accepted for publication in ApJ
Preprint typeset using LaTeX style emulateapj v. 5/2/11

arXiv:1511.09132v2 [astro-ph.GA] 15 Jan 2016

CLUSTERING PROPERTIES AND HALO MASSES FOR CENTRAL GALAXIES IN THE LOCAL UNIVERSE

Lixin Wang[1], Cheng Li[1,2], and Y. P. Jing[3]

Accepted for publication in ApJ

ABSTRACT

We investigate the clustering and dark matter halo mass for a sample of ∼16,000 central galaxies selected from the SDSS/DR7 group catalog. We select subsamples of central galaxies on three two-dimensional planes, each formed by stellar mass (M_*) and one of the other properties including optical color ($g-r$), surface stellar mass density (μ_*) and central stellar velocity dispersion (σ_*). For each subsample we measure both the projected cross-correlation function ($w_p(r_p)$) relative to a reference galaxy sample, and an average mass of the host dark matter halos (M_h). For comparison we have also estimated the $w_p(r_p)$ for the full galaxy population and the subset of satellite galaxies in the same group catalog. We find that, for central galaxies, both $w_p(r_p)$ and M_h show strongest dependence on M_*, and there is no clear dependence on other properties when M_* is fixed. This result holds at all the masses considered ($M_* > 2\times10^{10}M_\odot$). This result provides strong support to the previously-adopted assumption that, for central galaxies, stellar mass is the galaxy property that is best indicative of the host dark halo mass. The full galaxy population and the subset of satellites show similar clustering properties in all cases. However, they are similar to the centrals only at high masses ($M_* \gtrsim 10^{11}M_\odot$). At low-mass ($M_* \lesssim 10^{11}M_\odot$), the clustering properties of the full population and the satellite galaxies differ from that of the centrals: the $w_p(r_p)$ increases with both σ_* and $g-r$ when M_* is fixed, and depends very weakly on M_* when σ_* or $g-r$ is fixed. At fixed M_*, the μ_* shows weak correlations with clustering amplitude (and halo mass in case of central galaxies). This is true for both centrals and satellites, and holds at all masses and scales except at r_p below a few Mpc and $M_* \lesssim 10^{11}M_\odot$, where the galaxies with higher surface density are more clustered. Our results suggest that it is necessary to consider central and satellite galaxies separately when studying the link between galaxies and dark matter halos. We discuss the implications of our results on the relative roles of halo mass and galaxy structure in quenching the star formation in central galaxies.

Subject headings: dark matter - galaxies: halos - large-scale structure - method: statistical

1. INTRODUCTION

In current galaxy formation models, galaxies form at the center of dark matter halos when gas is able to cool, condense and form stars (White & Rees 1978). At this stage the galaxy is called a *central galaxy*, and its growth is believed to be tightly linked with the growth of the host dark matter halo. Indeed, a tight correlation has been well established, both theoretically (e.g. Moster et al. 2010; Guo et al. 2010) and observationally (e.g. Mandelbaum et al. 2006; Yang et al. 2007; Li et al. 2012, 2013), between the total mass of stars in a central galaxy (stellar mass, M_*) and the dark matter mass of its host halo (M_h). At a later stage the central galaxy, together with its host dark halo, may be accreted into a larger halo, and consequently the galaxy becomes a *satellite galaxy* and its halo becomes a *subhalo* of the new system. As a result the galaxy will deviate to varying degrees from the stellar mass–halo mass relation of the central galaxies. In addition, environmental effects such as gas stripping by ram-pressure (Gunn & Gott 1972; Abadi et al. 1999) and tidal interactions (Toomre & Toomre 1972; Moore et al. 1996) occurring within the new system may effectively reduce the hot gas halo, and in some cases even the cold gas and stellar components of the satellite galaxy, thus making the correlation with halo mass even more loose. It is thus important to consider central and satellite galaxies separately when studying the physical link between galaxies and dark halos.

Over the past decade, extensive studies have attempted to determine the halo mass as a function of stellar mass (or stellar luminosity) for central galaxies using a variety of observational probes such as galaxy clustering, satellite kinematics, gravitational lensing and group/cluster catalogs. These studies have obtained a M_h–M_* relation that follows a double power-law form with a small scatter of ~ 0.16 dex in $\lg(M_*/M_\odot)$ at fixed M_h (e.g. Yang et al. 2003; Vale & Ostriker 2004; van den Bosch et al. 2004; Conroy et al. 2006; Mandelbaum et al. 2006; Wang et al. 2006, 2007; Yang et al. 2007; Baldry et al. 2008; More et al. 2009; Behroozi et al. 2010; Guo et al. 2010; Moster et al. 2010; Li et al. 2012; More et al. 2011; Li et al. 2013; Kravtsov et al. 2014). This relation has been widely-adopted to populate dark matter halos with galaxies in current physical/statistical models such as semi-analytic models (White & Frenk 1991; Kauffmann et al. 1997), halo occupation distribution models (Jing et al. 1998; Benson et al. 2000), and subhalo abundance matching models (Vale & Ostriker 2004).

Besides stellar mass, other galaxy properties such

wlixin@shao.ac.cn, leech@shao.ac.cn
[1] Shanghai Astronomical Observatory, 80 Nandan Road, Shanghai 200030, China
[2] Physics Department and Tsinghua Center for Astrophysics, Tsinghua University, Beijing, 100084, China
[3] Center for Astronomy and Astrophysics, Department of Physics, Shanghai Jiaotong University, Shanghai 200240, China

as color, star formation rate, morphology and internal structure are also found to be correlated with halo mass, as usually probed by galaxy clustering (e.g. Li et al. 2006a; Zehavi et al. 2011), halo occupation statistics (e.g. Yang et al. 2008), abundance matching (e.g. More et al. 2011), and weak lensing (e.g. Mandelbaum et al. 2006). In particular, the SDSS data have recently revealed that, when both central and satellite galaxies are considered, the galaxy-galaxy correlation function appears to be less dependent on galaxy stellar mass, when compared to the parameters quantifying the prominence of a central bulge in the galaxy, such as central stellar velocity dispersion (σ_*; Wake et al. 2012a). This phenomenon may be attributed to the population of satellite galaxies for which the environmental processes such as tidal stripping occurring within their halos have stronger effect on stellar mass than on central stellar velocity dispersion. When only considering central galaxies and when stellar mass is fixed, halo mass shows little dependence on both the properties indicative of star formation history (e.g. More et al. 2011) and the σ_*, as recently demonstrated in Li et al. (2013, hereafter L13). In L13, the dark matter halo mass was estimated for samples selected by M_* and σ_*, by modelling the redshift-space distortion in the group-galaxy cross correlation function. It was clearly shown that, for central galaxies in the local Universe, stellar mass is better than stellar velocity dispersion as an indicator of dark matter halo mass.

In the current paper we extend the work of L13 by considering two more galaxy properties: optical color index ($g-r$) and surface stellar mass density (μ_*). The $g-r$ is a parameter associated with the recent star formation history of the galaxy, whereas μ_* is related to galaxy structure. We will estimate both clustering and halo mass for subsamples selected on two-dimensional planes each formed by M_* and one of the three properties: $g-r$, μ_* and σ_*. In addition to analyzing the central galaxies, we will study the clustering properties of both the full galaxy population and the subset of satellite galaxies, and compare the results for the different populations. Through these analyses, we aim to answer the following questions:

- Is stellar mass the galaxy property that is most related to halo mass? How is stellar mass compared to the recent star formation history (as indicated by $g-r$), the structural properties (as quantified by μ_*) and the central stellar velocity dispersion (σ_*) in terms of linking galaxies with dark halos?
- Is the correlation of halo mass and clustering with galaxy properties always stronger when we consider central galaxies only? What are the relative contributions of centrals and satellites to the overall clustering of galaxies?

The paper is structured as follows. In §2 we describe the galaxy sample and the physical properties used in this work. In §4.1 we focus on central galaxies, presenting the co-dependence of clustering and halo mass on galaxy properties. In §4.2 we examine the clustering properties for the full galaxy population and the satellite galaxies. Finally, we summarize our results and discuss on the implications on the link between galaxies and dark matter halos, as well as the relative roles of halo mass and galaxy structure in quenching the star formation in central galaxies.

Throughout this paper we assume a cosmology model with the density parameter $\Omega_m = 0.27$ and the cosmological constant $\Omega_\Lambda = 0.73$, and a Hubble constant $H_0 = 100h$ km s^{-1}Mpc^{-1} with $h = 0.7$.

2. DATA

2.1. *Samples*

For this work we have constructed three samples: i) a sample of central galaxies based on the SDSS group catalog of Yang et al. (2007), ii) a reference sample of galaxies selected from the SDSS data release 7 (DR7 Abazajian et al. 2009), and iii) a random sample that has the same selection effects as the reference sample. Here we briefly describe these samples and refer the reader to our previous studies for more details: Li et al. (2012, hereafter L12) and L13.

Central galaxy sample:: Yang et al. (2007) constructed a group catalog by applying a modified version of the halo-based group-finding algorithm of Yang et al. (2005) to a sample of $\sim 6.4\times10^5$ galaxies that are in the redshift range $0.01 \le z \le 0.2$ and selected from `sample dr72` of the New York University Value-Added Galaxy Catalog (NYU-VAGC). The NYU-VAGC is a catalog of local galaxies from the SDSS/DR7, publicly available at http://sdss.physics.nyu.edu/vagc/, and is described in detail in Blanton et al. (2005b). Following L12 and L13 we restrict ourselves to a subset of the group catalog, which consists of $\sim 16,000$ group systems with the number of member galaxies $N_{\rm mem} \ge 3$ and the stellar mass of the central galaxy $M_* > 2\times10^{10}M_\odot$. We use the most massive galaxy member as the central galaxy of each group.

Reference galaxy sample:: The reference sample is a magnitude-limited galaxy catalog selected from the NYU-VAGC `sample dr72`, consisting of about half a million galaxies with $r < 17.6$, $-24 < M_{0.1r} < -16$ and $0.01 < z < 0.2$. Here, r is the r-band Petrosian apparent magnitude, corrected for Galactic extinction; $M_{0.1r}$ is the r-band Petrosian absolute magnitude, corrected for evolution and K-corrected to its value at $z = 0.1$.

Random sample:: The random sample is constructed from the reference sample itself following the method described in Li et al. (2006a). For each real galaxy in the reference sample, we generated 10 sky positions at random within the mask of the real sample, assigning to each of them the redshift of the real galaxy. The resulting random sample is expected to be unclustered but fills the same sky region and has the same position- and redshift-dependent effects as the real sample. Extensive tests in Li et al. (2006a) show that random samples constructed in this way are valid for clustering analyses, provided that the survey area is large enough and that the effective depth of the survey does not vary. Both requirements are met to good accuracy by our reference sample, which covers $\gtrsim 6000$ deg^2,

complete down to $r = 17.6$ and little affected by foreground dust over the entire survey footprint.

2.2. *Galaxy properties*

The galaxy properties needed for this work include stellar mass (M_*), surface stellar mass density (μ_*), optical color ($g-r$), and central stellar velocity dispersion (σ_*). We take the measurements of these properties from both the NYU-VAGC and the MPA/JHU SDSS database. The latter is publicly available at http://www.mpa-garching.mpg.de/SDSS/DR7/, and is described in detail in Brinchmann et al. (2004).

We use the optical color index defined by the g-band and r-band Petrosian magnitudes, which are corrected for Galactic extinction, and K-corrected to their values at $z = 0.1$ using the `kcorrect` code of Blanton et al. (2003).

A stellar mass accompanies the NYU-VAGC release for each galaxy in our group catalog and reference sample. This was estimated by Blanton & Roweis (2007) based on the spectroscopically-measured redshift of the galaxy and its "Petrosian" magnitude in the SDSS five bands, assuming a universal initial mass function of Chabrier (2003) form and implicitly correcting for dust attenuation. We have corrected the Petrosian mass to obtain a "total mass" using the SDSS model magnitudes as described in Appendix A of Guo et al. (2010). As demonstrated in Li & White (2009), the masses from Blanton & Roweis (2007) agree pretty well with those obtained from the simple, single color estimator of Bell et al. (2003), as well as those derived by Kauffmann et al. (2003) from a combination of SDSS photometry and spectroscopy. In order to test whether a different stellar mass definition will cause any bias in our analysis, we also use the stellar masses from the MPA/JHU database obtained by Kauffmann et al. (2003).

The surface stellar mass density of a galaxy is defined by $\mu_* = 0.5M_*/\pi R_{50,z}^2$, where $R_{50,z}$ is the radius enclosing half of the total light in z-band, and M_* is the "total" stellar mass from NYU-VAGC as described above.

The SDSS spectroscopy provides a stellar velocity dispersion (σ_*) in the central $3''$ of each galaxy. For disk-dominated galaxies, however, the σ_* thus obtained may be dominated by the global rotation rather than the random motion of stars. Therefore we obtain the central stellar velocity dispersion for our galaxies based on both photometry and spectroscopy from SDSS, but in different ways for galaxies with and without a prominent bulge. We determine the significance of bulge based on data from Simard et al. (2011) who have carried out a careful bulge/disk decomposition for ~ 1.1 million galaxies using the SDSS imaging. A galaxy is classified to have a prominent bulge if the bulge-to-total luminosity ratio $L_{bulge}/(L_{bulge}+L_{disk}) > 0.5$, or the effective radius of the bulge $R_{e,bulge} > 1.5''$. Otherwise, the galaxy is classified to have no/weak bulge component. Here the bulge/disk luminosities and radii are given by the $n = 4$ bulge + disk fitting model performed to the SDSS r-band image (see Simard et al. 2011 for detailed description of the model). According to the significance of bulge and the signal-to-noise (S/N) of the SDSS spectrum, we divide the galaxies into three classes, and obtain σ_* in different ways for different classes.

- For those galaxies with both a prominent bulge and a high S/N spectrum (r-band S/N>10), we directly use the σ_* measurement provided in the MPA/JHU database. Following previous studies we have corrected the σ_* of a galaxy to an aperture of its effective radius, adopting the relation found by Jorgensen et al. (1995): $\sigma_{*,\rm corr}/\sigma_{*,\rm fib} = (8\times r_{\rm fib}/R_{50,r})^{0.04}$, where $r_{\rm fib} = 1.5''$ and $R_{50,r}$ is the radius enclosing half of the total light in r-band. At $\sigma_* > 100{\rm kms}^{-1}$ where we perform this study, about 53% of our galaxies fall into this class.

- For the galaxies with a prominent bulge but a low-quality spectrum with S/N≤ 10, we assign a σ_* to each galaxy according to the correlation between σ_* and bulge luminosity $L_{\rm bulge}$, which is given by the galaxies in the above class. In practice, we bin all the galaxies from the above class into narrow intervals of $L_{\rm bulge}$, and for a given interval we obtain the distribution function of σ_* according to which we randomly generate a σ_* for the galaxies falling in this interval. In this way both the median relation of σ_*-$L_{\rm bulge}$ in the high-S/N sample and the scatter of the galaxies around the median relation are reproduced in the low-S/N sample. At $\sigma_* > 100{\rm kms}^{-1}$ only a tiny fraction (1.4%) of galaxies fall into this class. Our tests here show that dropping this class would not impact our results in this paper.

- For the galaxies without a prominent bulge, we follow previous studies (e.g. Sheth et al. 2003; Chae 2010) to estimate σ_* from converting the circular velocity v_c: $\sigma_* = v_c/\sqrt{2}$, assuming the singular isothermal sphere (SIS) model for the total mass distribution of a galaxy. The circular velocity is given by the Tully-Fisher relation: $\log_{10} v_c = (-0.135\pm0.006)(M_r - M_r^*) + (2.210\pm0.006)$ with $M_r^* - 5\log_{10} h = -20.332$ and a dispersion of 0.063 ± 0.005, which was found by Pizagno et al. (2007) for the SDSS r-band. At $\sigma_* > 100{\rm kms}^{-1}$ a fraction of 45.6% galaxies fall into this class.

We would like to point out that, although we have obtained the central σ_* differently for different morphologies, our results to be presented below are essentially insensitive to the σ_* measurements. We have repeated all the analyses using the σ_* measured directly from the SDSS spectra, obtaining exactly the same conclusions. A part of these analyses is presented in Appendix of this paper.

3. METHODOLOGY

Detailed description of our methods for measuring galaxy clustering and dark matter halo masses can be found in our previous papers (Li et al. 2006a,b, 2012). In this section we briefly describe these methods. Following these papers we estimate errors on all the measurements in the current work using the bootstrap resampling technique (Barrow et al. 1984).

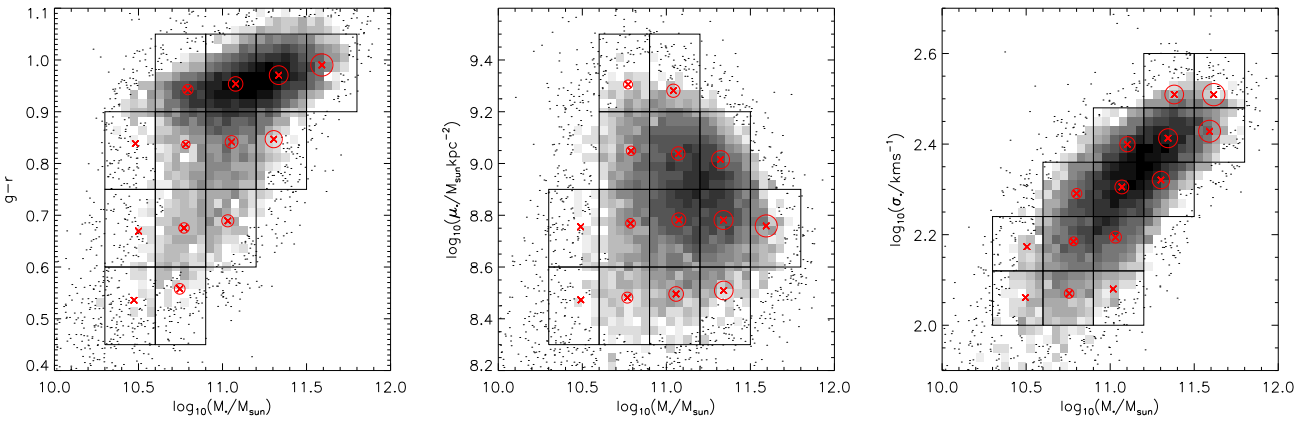

FIG. 1.— Distribution of the central galaxies in the SDSS/DR7 galaxy group catalog in the plane of (from left to right) stellar mass (M_*) versus optical color ($g-r$), M_* versus surface stellar mass density (μ_*), and M_* versus central stellar velocity dispersion (σ_*). Closed boxes indicate the subsamples analyzed in this paper, while the red cross in each box denotes the average of the sample galaxies. The red circle indicates the estimated halo mass (M_h), with the size of the circles being scaled by $\lg(M_h/M_\odot)$.

3.1. *Two-point cross-correlation function*

In this work we use two-point cross-correlation function (2PCCF) to quantify the clustering of our galaxies. For a given sample of galaxies (`Sample Q`), this is measured with respect to the reference galaxy sample constructed above (`Sample G`), over scales from a few tens of kpc up to a few tens of Mpc. On scales larger than a few Mpc, the amplitude of the 2PCCF provides a measure of the average mass for the dark matter halos that host the sampled galaxies. First, the redshift-space 2PCCF, $\xi^{(s)}(r_p,\pi)$, between `Sample Q` and `G`, is estimated by

$$\xi^{(s)}(r_p,\pi)=\frac{N_R}{N_G}\frac{QG(r_p,\pi)}{QR(r_p,\pi)}-1. \qquad (1)$$

Here, N_R and N_G are the number of galaxies in the random sample (`Sample R`) and in `Sample G`; r_p and π are the pair separations perpendicular and parallel to the line of sight; $QG(r_p,\pi)$ and $QR(r_p,\pi)$ are the counts of cross pairs between `Sample Q` and `G`, and between `Sample Q` and `R`. The projected 2PCCF is then obtained by integrating $\xi^{(s)}(r_p,\pi)$ over π:

$$w_p(r_p)=\int_{-\infty}^{+\infty}\xi(r_p,\pi)d\pi=\sum\xi(r_p,\pi_i)\Delta\pi_i. \qquad (2)$$

The summation for computing $w_p(r_p)$ runs from $\pi_1=-39.5h^{-1}$Mpc to $\pi_{80}=39.5h^{-1}$Mpc, with $\Delta\pi_i=1h^{-1}Mpc$. We correct the effect of fiber collisions using the method detailed in Li et al. (2006b).

3.2. *Dark matter halo mass of central galaxies*

For a given sample of central galaxies, we begin by estimating the redshift-space 2PCCF $\xi^{(s)}(r_p,\pi)$ and the projected 2PCCF $w_p(r_p)$ in the same way as described above. We then obtain the 2PCCF in real space, $\xi_{cg}(r)$, by the Abel transform of the $w_p(r_p)$. Next, the one-dimensional velocity dispersion profile (VDP) of satellite galaxies around the centrals is estimated by comparing $\xi^{(s)}(r_p,\pi)$ with $\xi_{cg}(r)$, through modeling the redshift-space distortion in $\xi^{(s)}(r_p,\pi)$.

In order to estimate an average mass for the dark matter halos that host these central galaxies, we have calibrated the relationship between the one-dimensional velocity dispersion and the dark matter halo mass, by applying the same method to N-body cosmological simulations. Finally, based on this relationship, we determine an average halo mass for the sample of central galaxies from their one-dimensional velocity dispersion.

It was demonstrated in L12 that the halo mass thus estimated for central galaxies of given luminosity agrees very well with that obtained by Mandelbaum et al. (2006) by stacking the weak lensing signals of SDSS galaxies. We have also compared the halo mass versus stellar mass relation obtained from our method with that in Zu & Mandelbaum (2015) and Mandelbaum et al. (2015), which were measured from galaxy-galaxy lensing but had smaller statistical errors and better mass modelling compared to Mandelbaum et al. (2006). Detailed description of our methodology, as well as comparisons with previous work and tests on the calibration, can be found in L12.

4. RESULTS

4.1. *Clustering and halo mass of central galaxies*

We begin with the central galaxies in our group catalog, estimating their redshift-space clustering and dark matter halo mass as function of their physical properties including stellar mass (M_*), optical color ($g-r$), surface stellar mass density (μ_*) and central stellar velocity dispersion (σ_*). To this end, we have selected a number of subsamples on the plane of M_* versus each of the other parameters: $g-r$, μ_* and σ_*. The selection is shown in Figure 1, which displays all the central galaxies with small dots in each of the three planes, with the subsamples in each plane enclosed by the black boxes. The average values of the two parameters for the selection is marked with a cross for each subsample. This selection scheme gives us at least two intervals in one parameter when the other is limited to a given interval, thus allowing us to study the dependence of clustering and halo mass on one of the two parameters while fixing the other.

Figure 2 presents the measurements of $w_p(r_p)$ for the

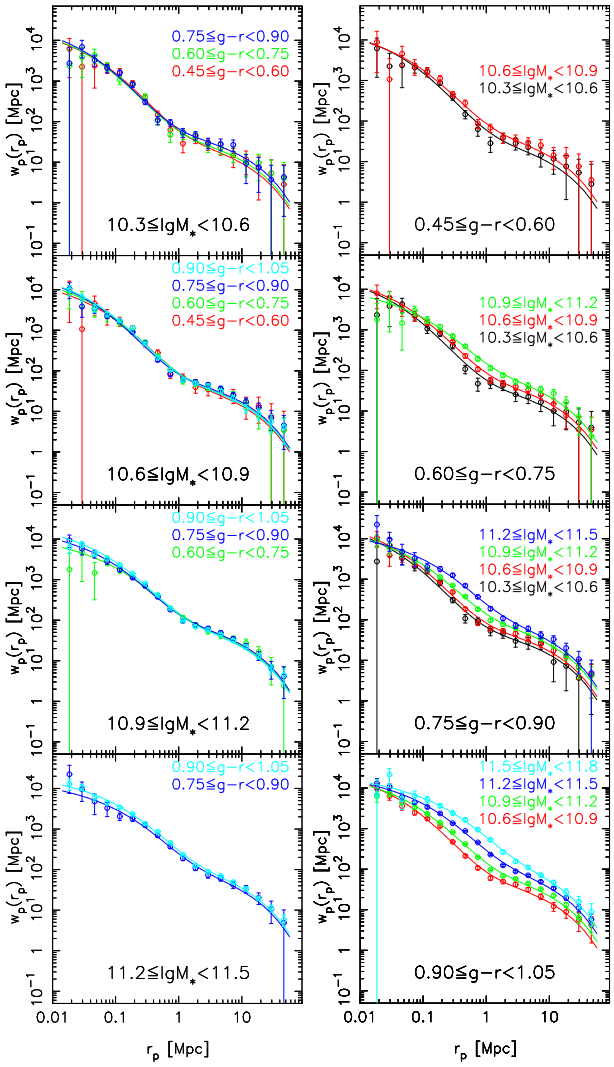

FIG. 2.— Projected cross-correlation function between subsamples of central galaxies and the reference galaxy sample, for central galaxies of different stellar mass (M_*) and optical color ($g-r$), as indicated in each panel. Plotted in colored symbols with error bars are the results from the SDSS/DR7 galaxy group catalog, while the solid lines present the best-fit models (see the text for details).

subsamples of central galaxies selected on the M_* vs. $g-r$ plane. We plot the results for different $g-r$ subsamples but fixed M_* in the left-hand panels, and the results for different M_* subsamples but fixed $g-r$ in the right-hand panels. At fixed stellar mass and given projected separation r_p, $w_p(r_p)$ shows very weak or no dependence on $g-r$, and this result holds for all the masses ($10.3 < \lg(M_*/M_\odot) < 11.5$) and separations ($\sim 20\mathrm{kpc} < r_p < \sim 50\mathrm{Mpc}$) probed here. In contrast, the $w_p(r_p)$ at fixed $g-r$ presents strong dependence on stellar mass, in terms of both amplitude and slope. This effect is true for all the $g-r$ bins except the bluest color bin ($0.45 \leq g-r \leq 0.60$) where we have only two subsamples due to the relatively narrow range in stellar mass. At given $g-r$ and on scales between $\sim$ 100kpc and a few Mpc, the $w_p(r_p)$ amplitude increases, while its slope flattens with increasing M_*. As a result, the transition between the "one-halo" and "two-halo" regimes occur at larger radii for higher masses, indicating that high-mass centrals are hosted by dark matter halos with larger virial radii (thus higher dark matter masses) when compared to low-mass centrals of the same $g-r$ color.

We present the correlation of halo mass with stellar mass and color in Figure 3, where the halo mass (M_h) estimated for all the central galaxy subsamples is plotted against both M_* (left panel) and $g-r$ (right panel). For comparison we have done the same analysis for a set of subsamples selected by M_* without further dividing the galaxies in each subsample into intervals of $g-r$, as well as a set of $g-r$ subsamples without further dividing the galaxies in each subsample into M_* intervals. This analysis leads to an *average* relation between M_h and M_* (left panel), and between M_h and $g-r$ (right panel), which are plotted as triangles connected with a solid line in the figure. The figure shows that M_h is correlated with both M_* and $g-r$, but the correlation with M_* is apparently much stronger than the correlation with $g-r$, in terms of both the scatter and slope of the relations. The rms scatter of the different $g-r$ subsamples around the average relation between M_h and M_* is 26.1%, compared to 138% for the different M_* subsamples around the M_h–$(g-r)$ relation. The average relation between M_h and M_* can be roughly described by a straight line with a steep slope. In contrast, the average relation between M_h and $g-r$ shows a similarly steep (but more scattering) relation only for red galaxies with $(g-r) \gtrsim 0.7$. For central galaxies of bluer colors, the average halo mass is nearly constant at $\sim 3 \times 10^{12} M_\odot$, close to the halo mass of the Milky Way. We note that, in the stellar mass range of $10.6 \leq \lg(M_*/M_\odot) < 10.9$, the halo mass appears to even show a non-monotonic dependence on color (see the green symbols in the right-hand panel), with both blue and red galaxies being hosted by dark halos of mass $\lg(M_h/M_\odot) \approx 12.5$ and the galaxies with intermediate color ($0.75 \leq g-r < 0.9$) moving in slightly lighter halos ($\lg(M_h/M_\odot) \sim 12.3$).

Figure 4 and 5 present the $w_p(r_p)$ and M_h estimates for subsamples selected on the plane of M_* and μ_*, in the same format and with the same symbols as above. The results are quite similar to what are found from the previous two figures, in the sense that $w_p(r_p)$ and M_h at fixed μ_* show strong dependence on stellar mass, with little residual correlation with μ_* when M_* is fixed. The halo mass averaged over all stellar masses depends on μ_* in a complicated way: M_h increases with increasing μ_*, reaching a maximum of $\lg(M_h/M_\odot) \approx 13.4$ at $8.6 \leq \lg(\mu_*/M_\odot \mathrm{kpc}^{-2}) < 8.9$, before it declines and becomes constant at $\lg(\mu_*/M_\odot \mathrm{kpc}^{-2}) \gtrsim 9.2$. At given μ_*, the different M_* subsamples scatter by an order of 1-1.5 magnitude in halo mass, with an overall rms scatter of 155% around the average relation between M_h and M_*. For comparison, the rms scatter is only 19.7% for the μ_* subsamples around the M_h–μ_* relation.

Figure 6 and 7 present the measurements of $w_p(r_p)$ and halo mass for the subsamples selected on the M_*–σ_* plane. These results were presented in Figures 2 and 4 in L13, and are repeated here for completeness and comparison. Similarly, M_h varies little with σ_* at fixed M_*, but shows strong and tight correlation with M_* when σ_* is limited to a narrow range. The rms scatter is 15.2% (73.2%) for the subsamples of σ_* (M_*) around the average relation of M_h with M_* (μ_*).

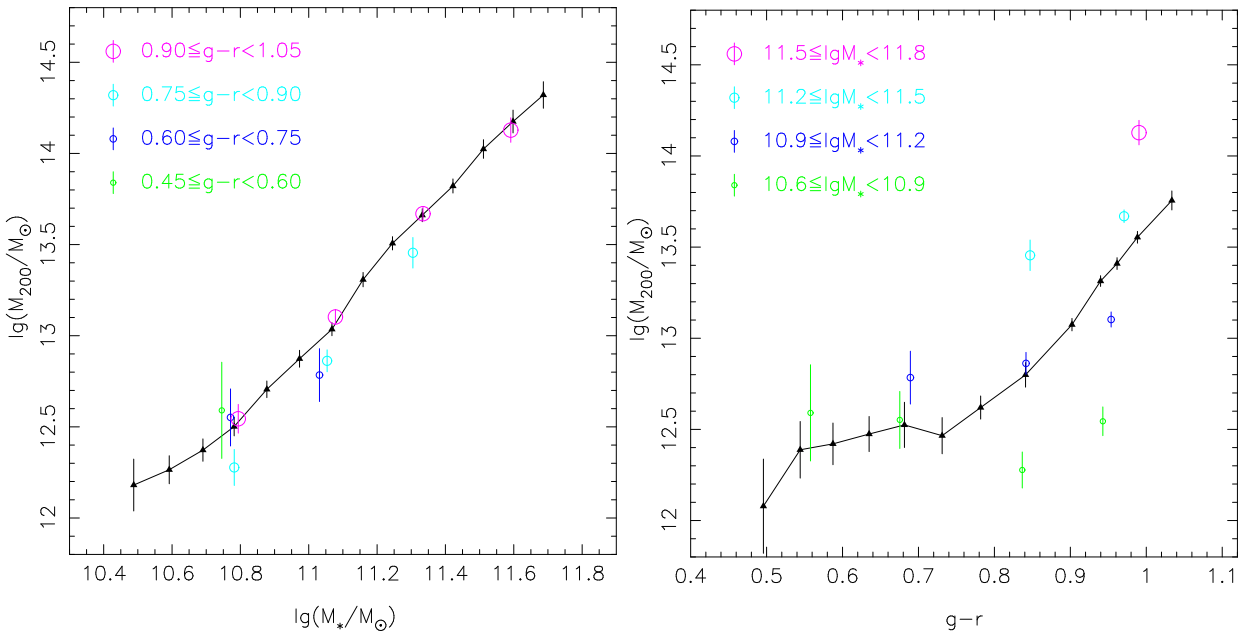

FIG. 3.— Dark matter halo mass as function of stellar mass (M_*, left panel) and optical color ($g-r$, right panel), measured for the central galaxies of the SDSS/DR7 groups. Plotted in colored symbols are the results for the subsamples selected on the M_* vs. $g-r$ plane as shown in Figure 1, while the triangles connected with the solid line are for samples selected only by M_* (left panel) or $g-r$ (right panel).

Figures 2 -7 echo the well-established tight correlation between the stellar mass and halo mass for central galaxies in dark matter halos. More importantly, these figures clearly show that the halo mass–stellar mass correlation holds tight even when σ_*, $g-r$ and μ_* are limited to a narrow range. We conclude that, among the physical parameters considered and for central galaxies with $\lg(M_*/M_\odot) > 10.3$, stellar mass is the galaxy property that is most closely correlated with dark matter halo mass. Both σ_* and $g-r$ are correlated with halo mass, with the former showing a steeper slope and a smaller scatter, but these correlations are largely driven by the correlation between halo mass and stellar mass. The μ_* is not correlated with halo mass for the central galaxies as a whole. At fixed stellar mass, the estimated halo mass shows very little correlation with μ_*, although we note that the halo mass appears to slightly decline with increasing μ_*, particularly in the lowest stellar mass bin ($10.6 \leq \lg(M_*/M_\odot) < 10.9$). The lack of correlation between μ_* and halo mass at fixed stellar mass implies that the mass–size relation of central galaxies, as well established by the large samples of both high-z and low-z galaxies, depends little on their host halo mass.

We summarize the co-dependence of halo mass on these physical parameters by indicating the estimated halo mass for each sample with a red circle in Figure 1, where the size of the circle is scaled linearly with $\lg(M_h/M_\odot)$. The strong correlation of halo mass with stellar mass, as well as the weak correlation with other parameters, can be visually identified in this figure. We conclude that, for central galaxies, the correlation of halo mass with stellar mass is still the tightest compared to the correlation with other properties.

4.2. *Clustering of the full galaxy population and satellite galaxies*

In this section we consider the full galaxy sample including both central and satellite galaxies. Since our methodology of estimating halo masses is applicable only for central galaxies, in what follows we will focus on measuring $w_p(r_p)$ for subsamples selected from the full sample, examining its co-dependence on the same set of physical properties analyzed above. Following the previous section, we select subsamples of galaxies on two-dimensional planes formed by M_* and one of the other properties including $g-r$, μ_* and σ_*, and for each subsample we then estimate the project CCF $w_p(r_p)$ with respect to the reference galaxy sample using the same method.

We start by measuring the $w_p(r_p)$ for subsamples selected on the M_*–σ_* plane. Figure 8 presents in the left panels the $w_p(r_p)$ measurements at fixed M_* but in different σ_* intervals, and in the right panels the measurements at fixed σ_* but different M_*. The ranges of M_* and σ_* used to select the subsamples are indicated in each panel. An overall impression from the figure is that, in almost all the panels we see systematic shift in $w_p(r_p)$ with increasing M_* (or σ_*) when σ_* (or M_*) is fixed. At fixed σ_*, the mass dependence of the clustering power is mainly seen at the highest stellar masses with $\lg(M_*/M_\odot) \gtrsim 11$. It is not surprising to note that such mass dependence is most pronounced in the highest σ_* bin (the bottom-right panel), which is expected given the known correlation between M_* and σ_*. At fixed M_*, the $w_p(r_p)$ increases with increasing σ_*, and similarly the effect appears to be stronger at higher σ_*.

These trends are more clearly seen in Figure 9 where we plot $w_p(r_p)$ measured at given projected separation r_p as a function of M_* for subsamples of different σ_* (left panels), and as a function of σ_* for subsamples of different M_* (right panels). In the left panels, both the weak mass dependence at low masses and the strong mass de-

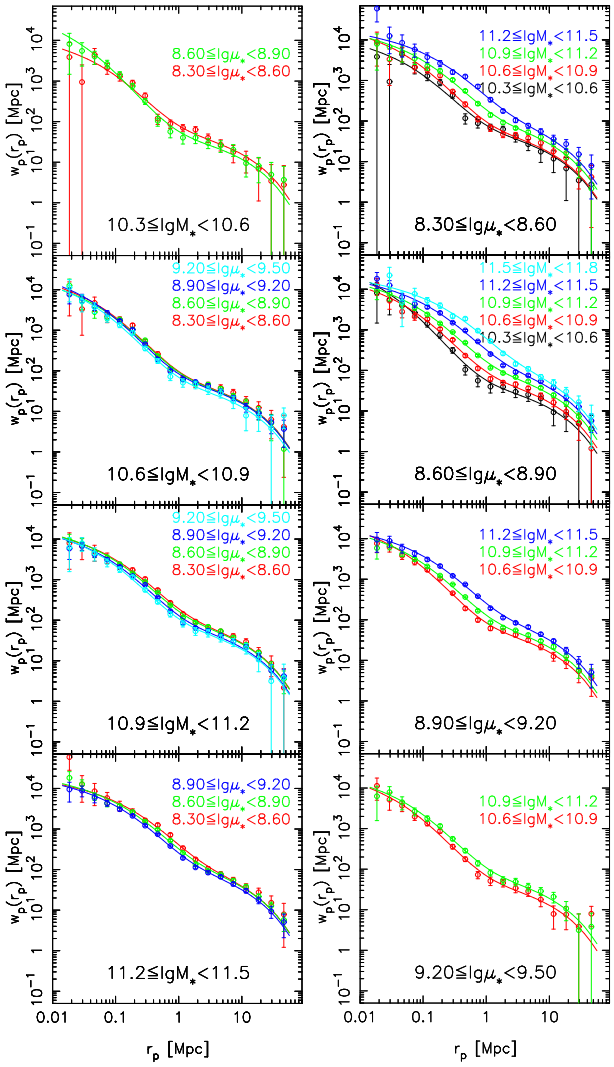

FIG. 4.— Projected cross-correlation function between subsamples of central galaxies and the reference galaxy sample, for central galaxies of different stellar mass (M_*) and surface stellar mass density (μ_*), as indicated in each panel. Plotted in colored symbols with error bars are the results from the SDSS/DR7 galaxy group catalog, while the solid lines present the best-fit models (see the text for details).

pendence at the massive end are apparently seen. On average the amplitude of $w_p(r_p)$ changes little when one goes from the lowest masses probed here ($M_* \gtrsim 10^{10} M_\odot$) up to $M_* \sim 10^{11} M_\odot$, before it increases remarkably at higher masses by at most a factor 2-3 depending on scale and σ_*. This result is consistent with the well-established behavior of the relative bias factor (b/b_*) of galaxy clustering measured in SDSS and other surveys, which depends weakly on stellar mass for galaxies with M_* below the characteristic mass of the stellar mass function but quickly increases at higher masses (e.g. Tegmark et al. 2004; Norberg et al. 2001; Zehavi et al. 2004; Li et al. 2006a). It is interesting to see that, at high masses with $M_* \gtrsim 10^{11} M_\odot$ and at intermediate to large scales with $r_p > 0.5 Mpc$, the $w_p(r_p)$ at fixed M_* shows little dependence on σ_*. In contrast, at lower masses and at all scales probed, the $w_p(r_p)$ at fixed M_* appears to depend on σ_*, with the effect being more marked at smaller r_p.

The $w_p(r_p)$ as a function of σ_*, plotted in the right-hand panels of the figure, presents similar behaviors to what we found in the left-hand panels, in the sense that the overall amplitude of $w_p(r_p)$ at given r_p increases with increasing σ_*, by a factor of 2-3 on average. However, when further dividing the galaxies by stellar mass, we find that the increase of $w_p(r_p)$ at high-σ_* ($\gtrsim 200$ kms^{-1}) is actually driven by the increase of M_* with σ_*. In this σ_* regime, the $w_p(r_p)$ shows little dependence on σ_*, while increasing dramatically with increasing M_* at given σ_*. At σ_* smaller than ~ 200 kms^{-1}, in contrast, it is the reverse that is in fact the case: the increase of $w_p(r_p)$ with σ_* seems to be driven by σ_* itself, an effect that is almost independent of M_*.

We now extend the analysis by examining the co-dependence of $w_p(r_p)$ on stellar mass and optical color ($g-r$). The $w_p(r_p)$ measurements for the subsamples selected by the two properties are presented in Figure 10. Overall the results are similar to what we see above for the subsamples selected by M_* and σ_*. At high masses ($>$ a few $\times 10^{11} M_\odot$) and red colors ($g-r \gtrsim 0.8$), the clustering amplitude depends strongly on M_* and weakly on $g-r$. Conversely, at lower masses and bluer colors, there is very weak or no dependence on stellar mass, and the dependence on color is clearly seen. These results are also broadly consistent with previous studies which measured the auto-correlation function of galaxies as a function of both stellar mass and color (e.g. Li et al. 2006a).

We further perform the same analysis to subsamples selected on the plane of M_* versus the surface stellar mass density (μ_*). Results are displayed in Figure 11. The behaviors of $w_p(r_p)$ on these figures are different from those on the previous figures. In most cases the clustering amplitude shows dependence only on stellar mass. There is no clear dependence on μ_* in all cases except at small scales with r_p below a few Mpc and at low stellar masses with $\lg(M_*/M_\odot) \lesssim 11$ (see the top two panels on the left-hand), where the clustering amplitude at fixed scale and mass increases with increasing μ_*.

We have analyzed the clustering properties for both the central galaxies in our sample and all the galaxies as a whole. For completeness we have also measured $w_p(r_p)$ for the satellite galaxies, by excluding the central galaxies from our sample and selecting subsamples of satellites on the same two-dimensional planes as above. We find that, overall, the $w_p(r_p)$ measured for the satellite galaxies depends on the galaxy properties in a way that is qualitatively quite similar to the $w_p(r_p)$ measured above for the full galaxy population, although for satellite galaxies we have to be limited to a smaller number of subsamples with more noisy measurements in some cases, due to the smaller number of satellite galaxies available in our sample.

The results in this section combine to reveal that, for galaxies as a whole, the clustering amplitude depends on both stellar mass and other properties considered, but in different ways for different types of galaxies. For massive galaxies with large M_* ($M_* \gtrsim 10^{11} M_\odot$), which also have large σ_*, $g-r$ and μ_*, the clustering is determined mainly on stellar mass, with little apparent dependence on other properties when M_* is fixed. At lower M_* the clustering depends on σ_* and $g-r$ at all scales in similar ways, and on μ_* only at scales smaller than a few Mpc. In any

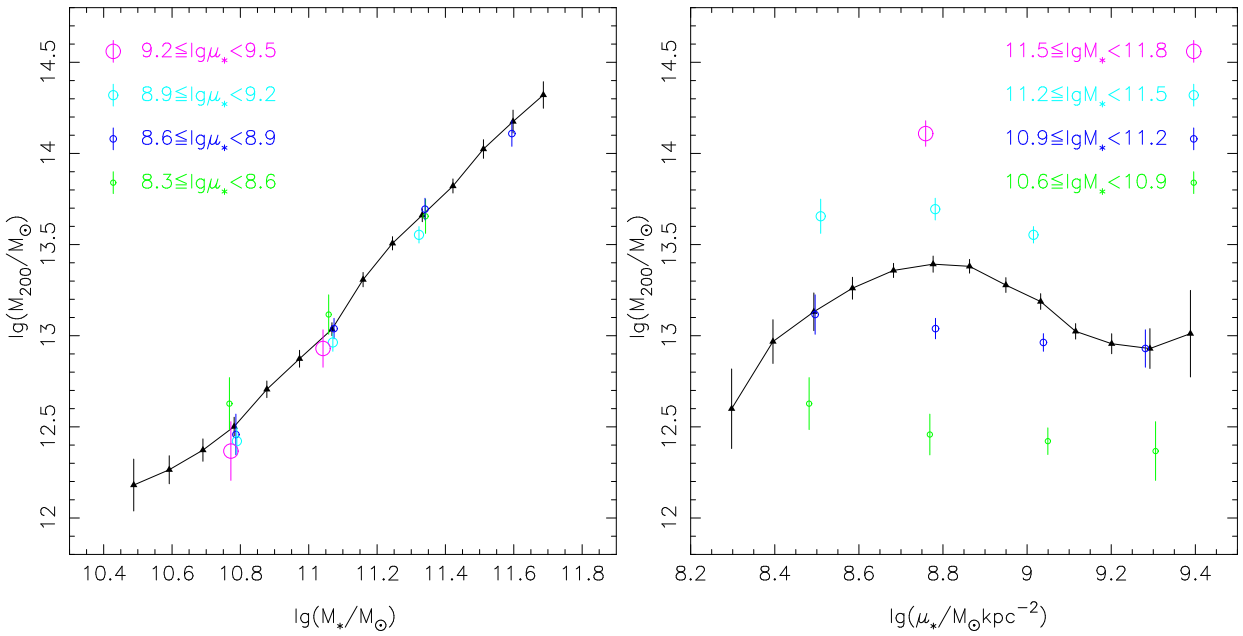

FIG. 5.— Dark matter halo mass as function of stellar mass (M_*, left panel) and surface stellar mass density (μ_*, right panel), measured for the central galaxies of the SDSS/DR7 groups. Plotted in colored symbols are the results for the subsamples selected on the M_* vs. μ_* plane as shown in Figure 1, while the triangles connected with the solid line are for samples selected only by M_* (left panel) or μ_* (right panel).

case, the clustering amplitude shows little dependence on M_* at lower masses, when one of the other properties is fixed. These results hold true when only considering satellite galaxies. This implies that the different clustering properties at lower masses, as seen in the central galaxy sample and the full sample, are mainly caused by the satellite galaxies which dominate the clustering at the low masses.

5. SUMMARY AND DISCUSSION

In this paper we have studied the clustering of both central and satellite galaxies in a large sample of ∼16,000 galaxy groups identified by Yang et al. (2007) from the SDSS/DR7, as well as the clustering of the full population including both centrals and satellites. In order to understand the co-dependence of clustering on stellar mass (M_*) and other properties, we have divided our galaxies into subsamples on two-dimensional planes each formed by M_* and one of the other properties including stellar velocity dispersion (σ_*), optical color ($g-r$) and surface stellar mass density (μ_*). For each subsample we then measure the projected cross-correlation functions $w_p(r_p)$ with respect to a reference sample consisting of about half a million galaxies, also selected from the SDSS/DR7. For each subsample of central galaxies, we have further estimated an average dark matter halo mass (M_h), by modelling the redshift distortion in the redshift-space cross-correlation function between the centrals and the reference galaxies. We have compared these measurements for the different populations, and for subsamples selected by different properties.

Our main conclusions can be summarized as follows.

1. For central galaxies, we find that both the clustering amplitude on scales larger than a few Mpc and the dark matter halo mass show strongest dependence on M_*, and there is no clear dependence on other properties when M_* is fixed. This result holds at all the stellar masses considered ($M_* > 2\times10^{10}M_\odot$). Our finding provides strong support to the commonly-adopted assumption that, for central galaxies, stellar mass is the galaxy property that is best indicative of the host dark halo mass.

2. The full galaxy population and the subset of satellites show similar clustering properties in all cases, which are similar to those of the central galaxies only at high-mass ($M_* \gtrsim 10^{11}M_\odot$).

3. At low-mass ($M_* \lesssim 10^{11}M_\odot$), the clustering properties of the full population and the satellite galaxies differ from those of the central galaxies: the clustering amplitude increases with both σ_* and $g-r$ when M_* is fixed, and depends very weakly on M_* when σ_* or $g-r$ is fixed.

4. At fixed M_*, the surface mass density μ_* shows weak correlations with clustering amplitude (and halo mass in case of central galaxies). This is true for both centrals and satellites, and holds at all masses and on all scales, except that at r_p below a few Mpc and $M_* \lesssim 10^{11}M_\odot$, the galaxies with higher surface density are more clustered.

The strong mass dependence of galaxy clustering at the high mass end has been well established in previous studies through measuring the auto-correlation function of galaxies in SDSS and other surveys (e.g. Tegmark et al. 2004; Norberg et al. 2001; Zehavi et al. 2004; Li et al. 2006a). The same effect is revealed in this work by the cross-correlation functions which depend strongly on stellar mass for galaxies more massive than $\sim 10^{11}M_\odot$. It is interesting that the effect holds even when the galaxies

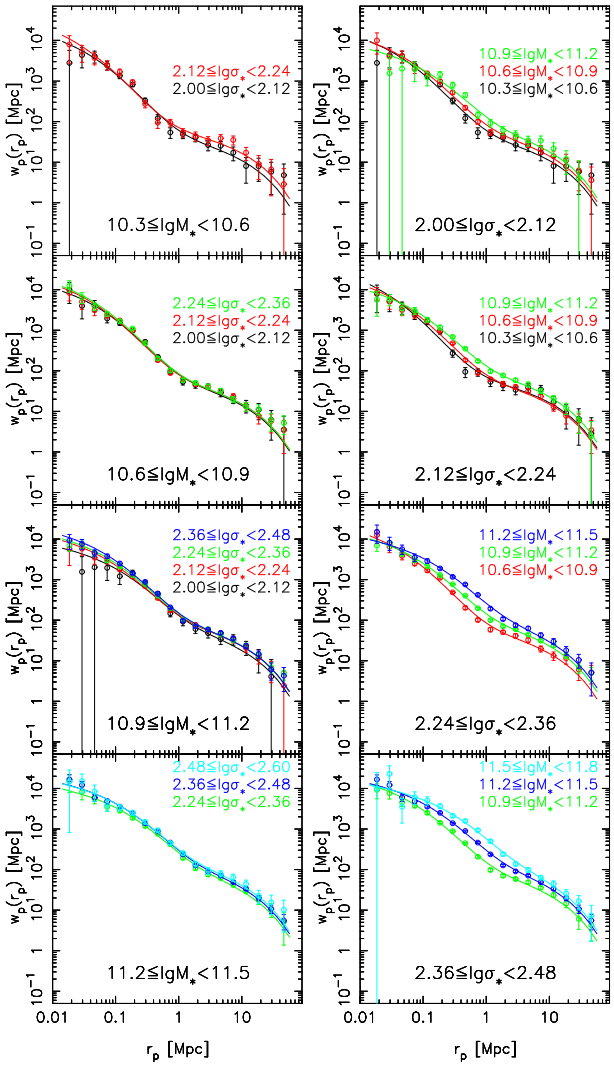

FIG. 6.— Projected cross-correlation function between subsamples of central galaxies and the reference galaxy sample, for central galaxies of different stellar mass (M_*) and central stellar velocity dispersion (σ_*), as indicated in each panel. Plotted in colored symbols with error bars are the results from the SDSS/DR7 galaxy group catalog, while the solid lines present the best-fit models (see the text for details).

are limited to narrow ranges in other properties. More interestingly, we find that the same effect at high-mass is seen when we divide the galaxies into centrals and satellites. It is clear that, for high-mass galaxies, stellar mass is the galaxy property that is most strongly correlated with clustering. This result was missing in the previous study by Wake et al. (2012a) who measured the $w_p(r_p)$ for the full galaxy population as a function of both M_* and σ_*, using the same statistic and similar data as in the current work. In order to understand the reason for the different results in Wake et al. and here, we have performed an additional analysis and present the results in the appendix (§A). It is shown that the lack of mass dependence at fixed σ_* in Wake et al. can be attributed to the too broad mass binning adopted, which smoothed out the mass dependence at the massive end.

At masses below $\sim 10^{11}M_\odot$, the clustering shows weak or no dependence on stellar mass, also in agreement with previous studies of the auto-correlation function of galaxies, and there is clear dependence on both σ_* and $g-r$ on all scales probed even when M_* is fixed. The dependence on σ_* at fixed mass found here is apparently consistent with Wake et al. (2012a). The similarity in the results for σ_* and $g-r$ may be reflecting the fact revealed by recent studies that σ_* is the best indicator of galaxy color when compared to other properties such as stellar mass, surface mass density and morphology (e.g. Wake et al. 2012b). The result for μ_* is somewhat different from that for σ_* and $g-r$, in the sense that the clustering amplitude shows dependence on μ_* only on scales smaller than a few Mpc, and this is true only for low-mass galaxies with $M_* \lesssim 10^{11}M_\odot$. The lack of dependence on μ_* on large scales is again consistent with previous studies of auto-correlation functions (Li et al. 2006a), which are found to be independent of μ_* on scales above a few Mpc. Our result apparently agrees with early studies that examined the correlation of local environment with galaxy properties, finding color to be the galaxy property most predictive of the local environment and structural parameters to be almost independent of local density at fixed stellar mass (e.g. Blanton et al. 2005a; Kauffmann et al. 2004).

In L13 we concluded that, when compared to stellar velocity dispersion, the stellar mass is better for indicating the host dark halo mass of central galaxies. In this work we have extended this work by including $g-r$ and μ_*, which are the galaxy parameters sensitive to recent star formation history and internal structure. We find that stellar mass is still the galaxy property that is most tightly correlated with dark halo mass (and clustering). Therefore, it is clear that the stellar mass is better than other properties such as stellar velocity dispersion, optical color and surface mass density, in terms of linking central galaxies with their host halo. One may question the reliability of taking the most massive galaxy as the central galaxy of groups (e.g. Skibba et al. 2011) . However, a recent study of X-ray observations of nearby clusters of galaxies (von der Linden et al. 2014) has nicely shown that the typical offset is only 20 kpc between the brightest cluster galaxy (BCG) and X-ray centroid, and that measurements of weak lensing mass centered at BCGs agree well with those centered at X-ray centroids. This suggested that the BCGs (and similarly the most massive galaxy) are indeed very close to the potential center of clusters.

The full sample and the satellite population show similar clustering properties, which are similar to those of central galaxies only at high masses ($M_* \gtrsim 10^{11}M_\odot$). This confirms our previous conjecture that it is necessary to consider central and satellite galaxies separately when studying the link between galaxy and dark matter halos. The current work shows that the clustering of the two types of galaxies depends on the galaxy properties in different ways. Therefore, the behavior of clustering for a sample including both populations must strongly depends on the central/satellite fraction of the sample. It is thus not surprising that the stellar mass is always most related with clustering and halo mass at the massive end, where the sample is dominated by central galaxies. At lower masses, in contrast, the satellite fraction is larger and the result of the full sample is mainly reflecting the behavior of satellite galaxies.

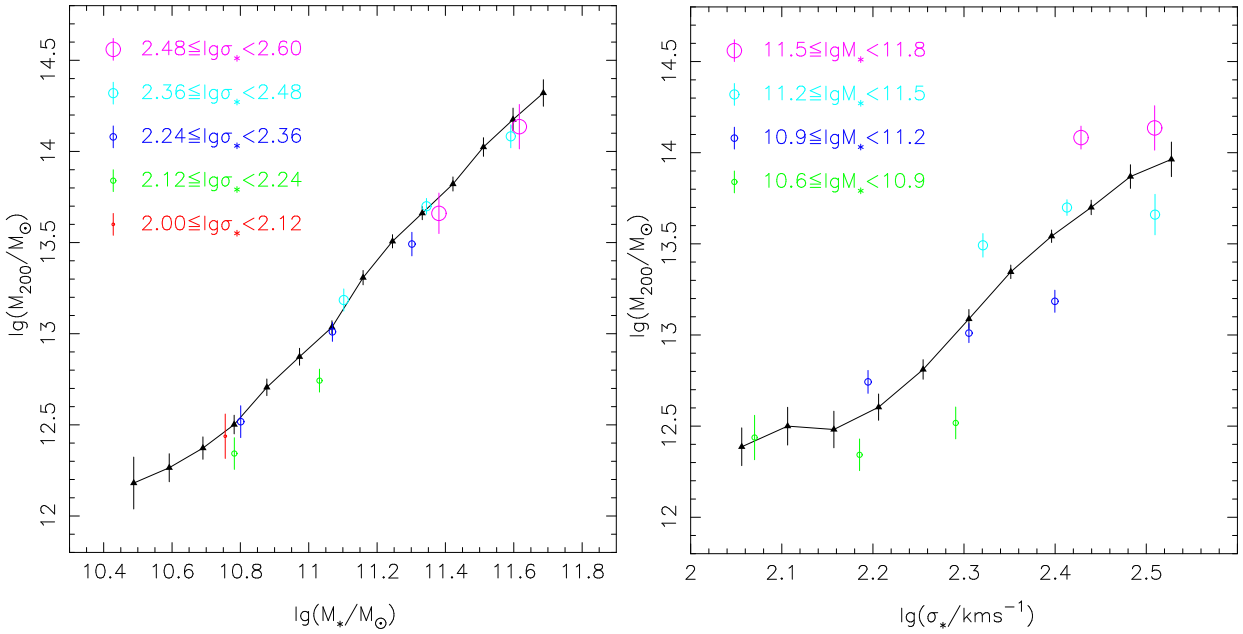

FIG. 7.— Dark matter halo mass as function of stellar mass (M_*, left panel) and central stellar velocity dispersion (σ_*, right panel), measured for the central galaxies of the SDSS/DR7 groups. Plotted in colored symbols are the results for the subsamples selected on the M_* vs. σ_* plane as shown in Figure 1, while the triangles connected with the solid line are for samples selected only by M_* (left panel) or σ_* (right panel).

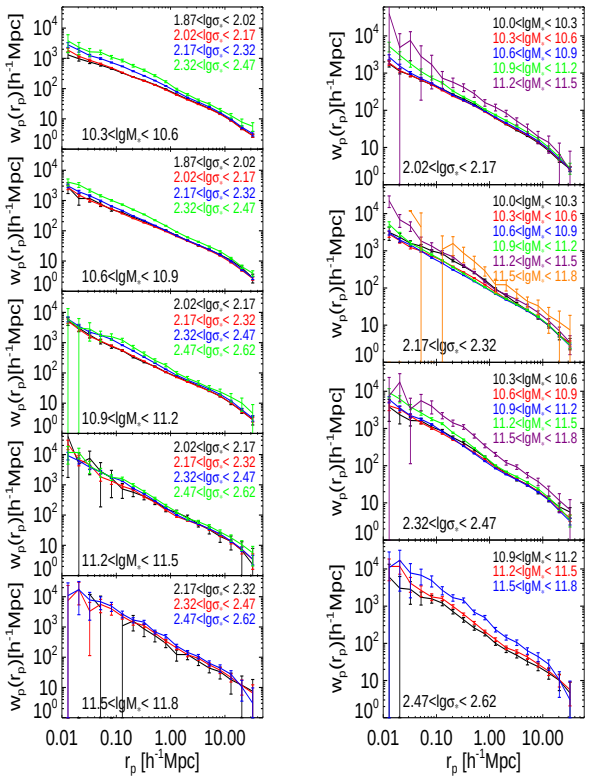

FIG. 8.— Projected cross-correlation function $w_p(r_p)$ of subsamples of galaxies selected by M_* and σ_*, with respect to the reference galaxy sample. Left panels show $w_p(r_p)$ measurements in different intervals of σ_* but fixed M_*. Right panels show the measurements for different M_* intervals but fixed σ_*.

Finally, we would like to point out that our results may be helpful for understanding the role of dark matter halos in quenching the star formation in central galaxies, a current topic that has been studied in depth by many authors, both observationally and theoretically. On one hand, theoretically the so-called "halo quenching" process is expected to be at work for central galaxies of massive halos reaching a critical halo mass of $\sim 10^{12}M_\odot$, where the infalling gas is shock-heated to the virial temperature and is no longer able to cool efficiently (e.g. Silk 1977; Rees & Ostriker 1977). On the other hand, recent studies of the correlations between galaxy color and structural parameters based on SDSS and high-z surveys have reached a well-established conclusion that the presence of a prominent central object such as a bulge is a necessary, but not sufficient condition for quenching the star formation in central galaxies (e.g. Kauffmann et al. 2006; Bell 2008; Franx et al. 2008; Bell et al. 2012; Cheung et al. 2012; Fang et al. 2013). This result supports the "morphology quenching" process proposed by Martig et al. (2009), in which the buildup of a central massive spheroid can effectively stabilize the gas disk from gravitationally collapsing and forming stars. Recently Fang et al. (2013) suggested a "two-step" picture in which both the halo quenching and morphology quenching processes play important roles. However, the two processes could be essentially the same process if σ_* turns out to be most correlated with dark matter halo mass. In that case, halo mass would be the driving parameter for both the growth of the bulge within the galaxy (as quantified by σ_*) and the gas heating in the host halo. This possibility can be ruled out according to our analysis which clearly show that the halo mass is more tightly correlated with M_* than with σ_*. Our result suggests that halo quenching and morphology quenching are two distinct processes, driven by different physical

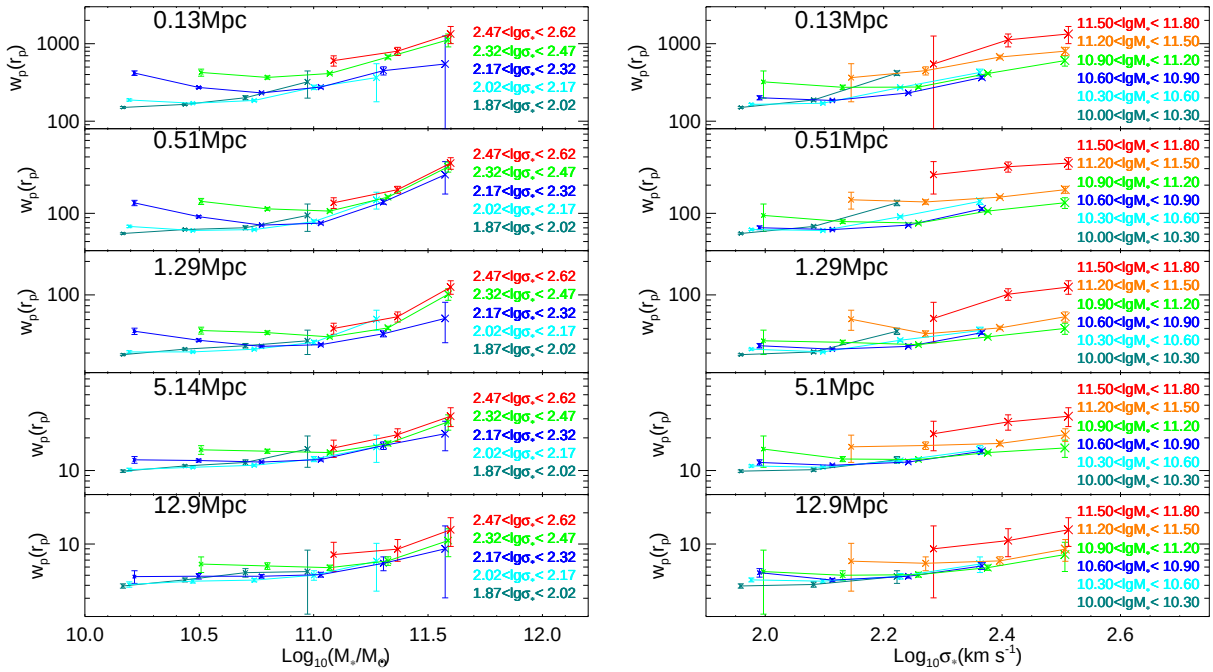

FIG. 9.— Projected cross-correlation function $w_p(r_p)$ measured at fixed scale as indicated in each panel, as a function of M_* (left panels) and σ_* (right panels). In the left panels, the colored symbols/lines are for different σ_* intervals but fixed M_*, and those in the right panels are for different M_* intervals but fixed σ_*.

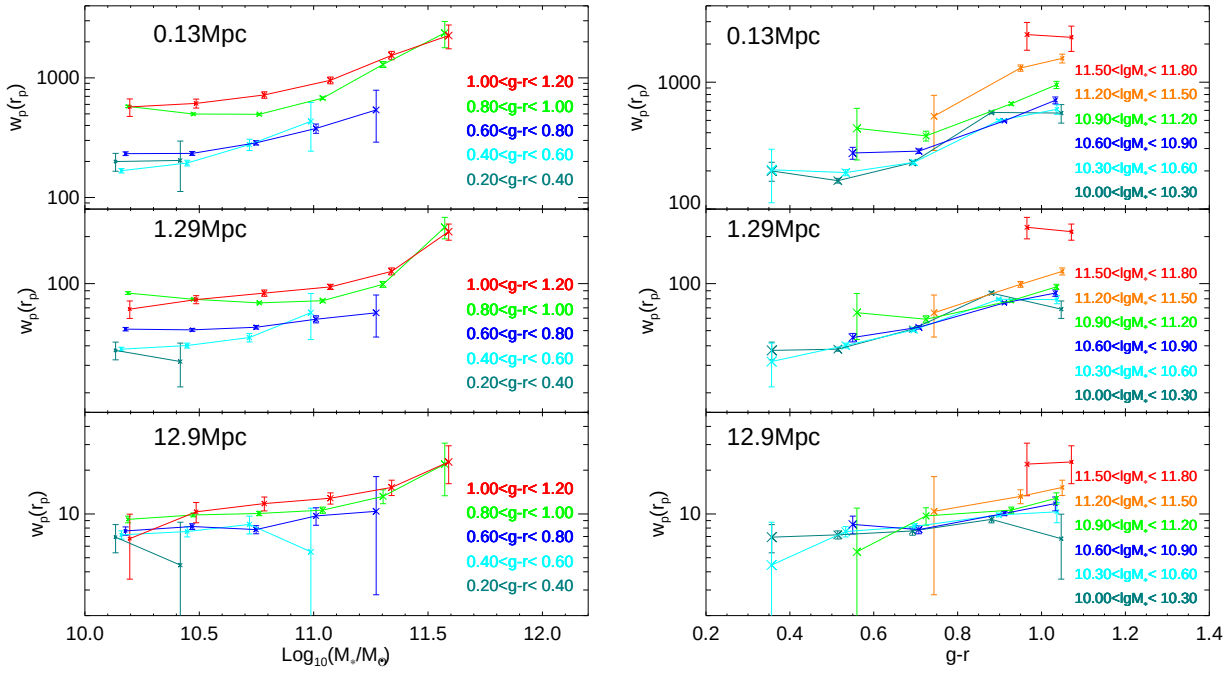

FIG. 10.— Projected cross-correlation function $w_p(r_p)$ measured at fixed scale as indicated in each panel, as a function of M_* for subsamples of different $g-r$ (left panels) and as a function of $g-r$ for subsamples of different M_* (right panels).

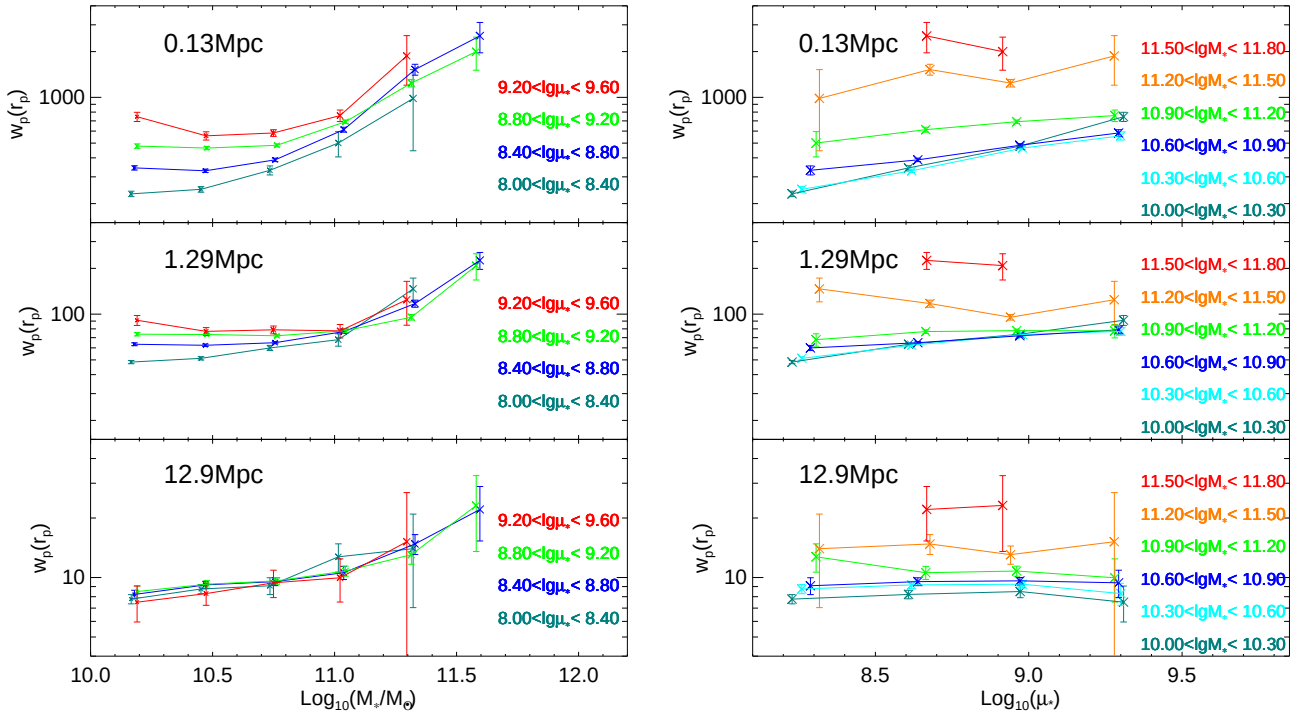

FIG. 11.— Projected cross-correlation function $w_p(r_p)$ measured at different scales as indicated, as a function of M_* for subsamples of different μ_* (left panels), and as a function of μ_* for subsamples of different M_* (right panels).

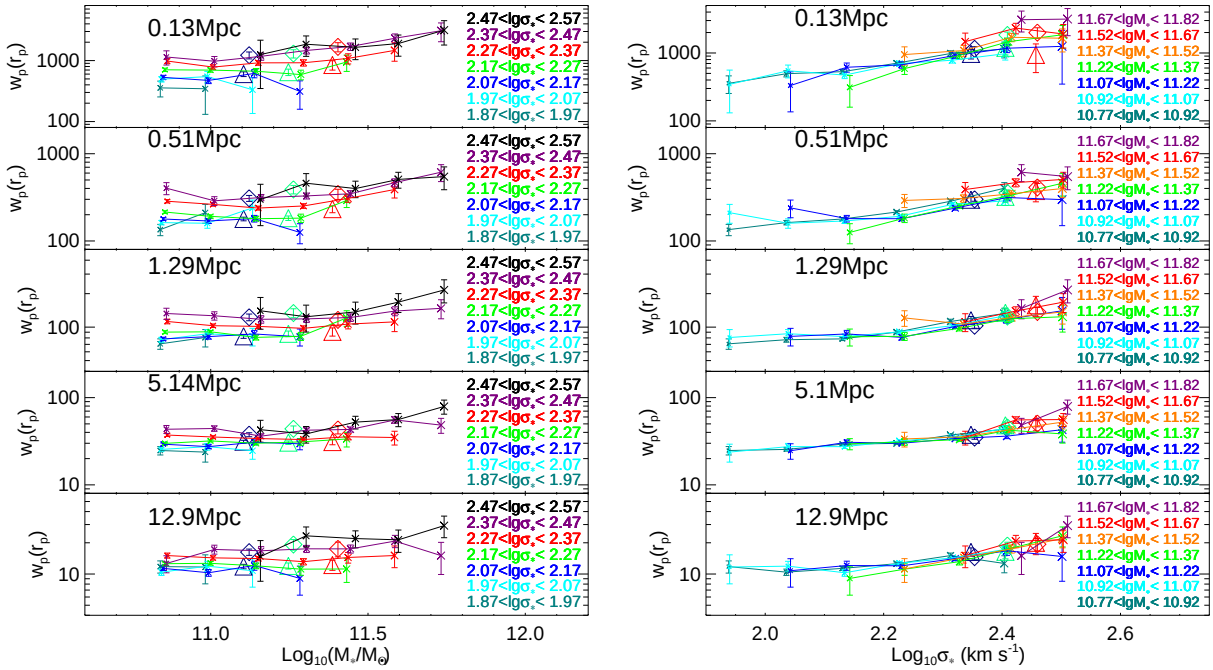

FIG. 12.— Same as the previous figure, except that we use stellar mass estimates and stellar velocity dispersion estimates from the MPA/JHU database following Wake et al. (2012a), when dividing our galaxies into subsamples of M_* and σ_*. Large triangles and diamonds present the results for subsamples selected with wider binning, adopting the same M_* and σ_* ranges as in Wake et al. (2012a).

processes and parameters.

We're grateful to the referee for the helpful comments. This work is supported by National Key Basic Research Program of China (No. 2015CB857004), NSFC (Grant No. 11173045, 11233005, 11325314, 11320101002) and the Strategic Priority Research Program "The Emergence of Cosmological Structures" of CAS (Grant No. XDB09000000).

Funding for the SDSS and SDSS-II has been provided by the Alfred P. Sloan Foundation, the Participating Institutions, the National Science Foundation, the U.S. Department of Energy, the National Aeronautics and Space Administration, the Japanese Monbukagakusho, the Max Planck Society, and the Higher Education Funding Council for England. The SDSS Web Site is http://www.sdss.org/. The SDSS is managed by the Astrophysical Research Consortium for the Participating Institutions. The Participating Institutions are the American Museum of Natural History, Astrophysical Institute Potsdam, University of Basel, University of Cambridge, Case Western Reserve University, University of Chicago, Drexel University, Fermilab, the Institute for Advanced Study, the Japan Participation Group, Johns Hopkins University, the Joint Institute for Nuclear Astrophysics, the Kavli Institute for Particle Astrophysics and Cosmology, the Korean Scientist Group, the Chinese Academy of Sciences (LAMOST), Los Alamos National Laboratory, the Max-Planck-Institute for Astronomy (MPIA), the Max-Planck-Institute for Astrophysics (MPA), New Mexico State University, Ohio State University, University of Pittsburgh, University of Portsmouth, Princeton University, the United States Naval Observatory, and the University of Washington.

APPENDIX

EXAMINING THE EFFECT OF DIFFERENT DATA SETS AND SAMPLE SELECTIONS

Here we present an additional analysis which attempts to examine the robustness of our results to the different definitions/estimations of stellar mass and stellar velocity dispersion, as well as to understand why the previous work by Wake et al. (2012a) led to different conclusions. For the first purpose, we use M_* and σ_* estimates from the MPA/JHU database, the same data as used by Wake et al. (2012a), and we repeat the analysis as done in the main text, selecting subsamples of the full galaxy population on the two-dimensional plane of M_* and σ_* with exactly the same binning scheme. The $w_p(r_p)$ measurements are presented in Figure 12. Comparing this figure and Figure 9, our conclusion remains unchanged regarding the co-dependence of clustering on M_* and σ_*, although there are subtle differences in some cases. Again, we find the $w_p(r_p)$ to depend mainly on M_* at high masses and on σ_* at low masses.

Using the same data and the same statistic, Wake et al. (2012a) reached a conclusion that is different from ours: there was no dependence of $w_p(r_p)$ on stellar mass at fixed σ_*, but dependence on σ_* was clearly seen at fixed M_*. However, the results from the two studies may not be comparable, as Wake et al. adopted much wider binning when selecting their subsamples. In order to examine the effect of the different selections, we follow Wake et al. to select 12 subsamples on the M_* vs. σ_* plane with the same binning scheme. The $w_p(r_p)$ measured at different scales as a

function of the median M_* (left panels) or the median σ_* (right panels) of these subsamples are plotted in Figure 12 as large triangles and diamonds. The results are in good agreement with Wake et al.: the clustering amplitude at given r_p shows strong dependence on σ_* at fixed M_* (see the comparison between triangles and diamonds in the left panels), and does not depend on M_* at fixed σ_* for scales beyond ~ 0.5 Mpc (see the comparison between triangles and diamonds in the bottom three panels at the right hand). Comparing these subsamples with the subsamples selected with finner binning, we find that the 6 subsamples in the left panels are dominated by galaxies of relatively low masses ($\lg(M_*/M_\odot) \lesssim 11.5$), a regime where the mass dependence of galaxy clustering is weak as discussed above. The mass dependence can only be seen at the highest masses, and can be easily hidden if the sample being considered covers a wide range of stellar mass. Regarding the 6 subsamples in the right panels, we find that these subsamples are biased to relatively large σ_*, but none of them are representative of the galaxies with the highest σ_*, only at which the clustering amplitude shows dependence on M_* at fixed σ_*. Therefore, our analysis here explains why Wake et al. failed to detect a mass dependence at fixed stellar velocity dispersion, which can be simply attributed to the too broad binning in both M_* and σ_* adopted in their sample selection.

REFERENCES

Abadi, M. G., Moore, B., & Bower, R. G. 1999, MNRAS, 308, 947
Abazajian, K. N., Adelman-McCarthy, J. K., Agüeros, M. A., Allam, S. S., Allende Prieto, C., An, D., Anderson, K. S. J., Anderson, S. F., & et al. 2009, ApJS, 182, 543
Baldry, I. K., Glazebrook, K., & Driver, S. P. 2008, MNRAS, 388, 945
Barrow, J. D., Bhavsar, S. P., & Sonoda, D. H. 1984, MNRAS, 210, 19P
Behroozi, P. S., Conroy, C., & Wechsler, R. H. 2010, ApJ, 717, 379
Bell, E. F. 2008, ApJ, 682, 355
Bell, E. F., McIntosh, D. H., Katz, N., & Weinberg, M. D. 2003, ApJS, 149, 289
Bell, E. F., van der Wel, A., Papovich, C., Kocevski, D., Lotz, J., McIntosh, D. H., Kartaltepe, J., Faber, S. M., & et al. 2012, ApJ, 753, 167
Benson, A. J., Cole, S., Frenk, C. S., Baugh, C. M., & Lacey, C. G. 2000, MNRAS, 311, 793
Blanton, M. R., Brinkmann, J., Csabai, I., Doi, M., Eisenstein, D., Fukugita, M., Gunn, J. E., Hogg, D. W., & et al. 2003, AJ, 125, 2348
Blanton, M. R., Eisenstein, D., Hogg, D. W., Schlegel, D. J., & Brinkmann, J. 2005a, ApJ, 629, 143
Blanton, M. R. & Roweis, S. 2007, AJ, 133, 734
Blanton, M. R., Schlegel, D. J., Strauss, M. A., Brinkmann, J., Finkbeiner, D., Fukugita, M., Gunn, J. E., Hogg, D. W., & et al. 2005b, AJ, 129, 2562
Brinchmann, J., Charlot, S., White, S. D. M., Tremonti, C., Kauffmann, G., Heckman, T., & Brinkmann, J. 2004, MNRAS, 351, 1151
Chabrier, G. 2003, PASP, 115, 763
Chae, K.-H. 2010, MNRAS, 402, 2031
Cheung, E., Faber, S. M., Koo, D. C., Dutton, A. A., Simard, L., McGrath, E. J., Huang, J.-S., Bell, E. F., & et al. 2012, ApJ, 760, 131
Conroy, C., Wechsler, R. H., & Kravtsov, A. V. 2006, ApJ, 647, 201
Fang, J. J., Faber, S. M., Koo, D. C., & Dekel, A. 2013, ApJ, 776, 63
Franx, M., van Dokkum, P. G., Schreiber, N. M. F., Wuyts, S., Labbé, I., & Toft, S. 2008, ApJ, 688, 770
Gunn, J. E. & Gott, III, J. R. 1972, ApJ, 176, 1
Guo, Q., White, S., Li, C., & Boylan-Kolchin, M. 2010, MNRAS, 404, 1111
Jing, Y. P., Mo, H. J., & Börner, G. 1998, ApJ, 494, 1
Jorgensen, I., Franx, M., & Kjaergaard, P. 1995, MNRAS, 273, 1097
Kauffmann, G., Heckman, T. M., De Lucia, G., Brinchmann, J., Charlot, S., Tremonti, C., White, S. D. M., & Brinkmann, J. 2006, MNRAS, 367, 1394
Kauffmann, G., Heckman, T. M., White, S. D. M., Charlot, S., Tremonti, C., Brinchmann, J., Bruzual, G., Peng, E. W., & et al. 2003, MNRAS, 341, 33
Kauffmann, G., Nusser, A., & Steinmetz, M. 1997, MNRAS, 286, 795
Kauffmann, G., White, S. D. M., Heckman, T. M., Ménard, B., Brinchmann, J., Charlot, S., Tremonti, C., & Brinkmann, J. 2004, MNRAS, 353, 713
Kravtsov, A., Vikhlinin, A., & Meshscheryakov, A. 2014, ArXiv e-prints
Li, C., Jing, Y. P., Mao, S., Han, J., Peng, Q., Yang, X., Mo, H. J., & van den Bosch, F. 2012, ApJ, 758, 50
Li, C., Kauffmann, G., Jing, Y. P., White, S. D. M., Börner, G., & Cheng, F. Z. 2006a, MNRAS, 368, 21
Li, C., Kauffmann, G., Wang, L., White, S. D. M., Heckman, T. M., & Jing, Y. P. 2006b, MNRAS, 373, 457
Li, C., Wang, L., & Jing, Y. P. 2013, ApJ, 762, L7
Li, C. & White, S. D. M. 2009, MNRAS, 398, 2177
Mandelbaum, R., Seljak, U., Kauffmann, G., Hirata, C. M., & Brinkmann, J. 2006, MNRAS, 368, 715
Mandelbaum, R., et al. 2015, MNRAS, submitted, arXiv:1509.06762
Martig, M., Bournaud, F., Teyssier, R., & Dekel, A. 2009, ApJ, 707, 250
Moore, B., Katz, N., Lake, G., Dressler, A., & Oemler, A. 1996, Nature, 379, 613
More, S., van den Bosch, F. C., Cacciato, M., Mo, H. J., Yang, X., & Li, R. 2009, MNRAS, 392, 801
More, S., van den Bosch, F. C., Cacciato, M., Skibba, R., Mo, H. J., & Yang, X. 2011, MNRAS, 410, 210
Moster, B. P., Somerville, R. S., Maulbetsch, C., van den Bosch, F. C., Macciò, A. V., Naab, T., & Oser, L. 2010, ApJ, 710, 903
Norberg, P., Baugh, C. M., Hawkins, E., Maddox, S., Peacock, J. A., Cole, S., Frenk, C. S., Bland-Hawthorn, J., & et al. 2001, MNRAS, 328, 64
Pizagno, J., Prada, F., Weinberg, D. H., Rix, H.-W., Pogge, R. W., Grebel, E. K., Harbeck, D., Blanton, M., Brinkmann, J., & Gunn, J. E. 2007, AJ, 134, 945
Rees, M. J. & Ostriker, J. P. 1977, MNRAS, 179, 541
Sheth, R. K., Bernardi, M., Schechter, P. L., Burles, S., Eisenstein, D. J., Finkbeiner, D. P., Frieman, J., Lupton, R. H., & et al. 2003, ApJ, 594, 225
Silk, J. 1977, ApJ, 211, 638
Simard, L., Mendel, J. T., Patton, D. R., Ellison, S. L., & McConnachie, A. W. 2011, ApJS, 196, 11
Skibba, R. A., van den Bosch, F. C., Yang, X., More, S., Mo, H., & Fontanot, F. 2011, MNRAS, 410, 417
Tegmark, M., Blanton, M. R., Strauss, M. A., Hoyle, F., Schlegel, D., Scoccimarro, R., Vogeley, M. S., Weinberg, D. H., & et al. 2004, ApJ, 606, 702
Toomre, A. & Toomre, J. 1972, ApJ, 178, 623
Vale, A. & Ostriker, J. P. 2004, MNRAS, 353, 189
van den Bosch, F. C., Norberg, P., Mo, H. J., & Yang, X. 2004, MNRAS, 352, 1302
von der Linden, A., Allen, M. T., Applegate, D. E., Kelly, P. L., Allen, S. W., Ebeling, H., Burchat, P. R., Burke, D. L., & et al. 2014, MNRAS, 439, 2
Wake, D. A., Franx, M., & van Dokkum, P. G. 2012a, ArXiv e-prints
Wake, D. A., van Dokkum, P. G., & Franx, M. 2012b, ApJ, 751, L44
Wang, L., Li, C., Kauffmann, G., & De Lucia, G. 2006, MNRAS, 371, 537
—. 2007, MNRAS, 377, 1419
White, S. D. M. & Frenk, C. S. 1991, ApJ, 379, 52
White, S. D. M. & Rees, M. J. 1978, MNRAS, 183, 341
Yang, X., Mo, H. J., & van den Bosch, F. C. 2003, MNRAS, 339, 1057
Yang, X., Mo, H. J., & van den Bosch, F. C. 2008, ApJ, 676, 248
Yang, X., Mo, H. J., van den Bosch, F. C., & Jing, Y. P. 2005, MNRAS, 356, 1293
Yang, X., Mo, H. J., van den Bosch, F. C., Pasquali, A., Li, C., & Barden, M. 2007, ApJ, 671, 153
Zehavi, I., Weinberg, D. H., Zheng, Z., Berlind, A. A., Frieman, J. A., Scoccimarro, R., Sheth, R. K., Blanton, M. R., & et al. 2004, ApJ, 608, 16
Zehavi, I., Zheng, Z., Weinberg, D. H., Blanton, M. R., Bahcall, N. A., Berlind, A. A., Brinkmann, J., Frieman, J. A., & et al. 2011, ApJ, 736, 59
Zu, Y. & Mandelbaum, R. 2015, MNRAS, 454, 1161